Self-assembly and Sensor Response of Photosynthetic Reaction Centers on Screen-printed Electrodes.

Vijayender Bhalla[+], Valter Zazubovich[*]

Department of Physics, Concordia University, 7141 Sherbrooke St. West, Montreal,Quebec H4B 1R6, Canada

Abstract

Photosynthetic reaction centers were immobilized onto gold screen-printed electrodes (Au-SPE) using a self-assembled monolayer (SAM) of mercaptopropionic acid (MPA) which was deliberately defective in order to achieve effective mediator transfer to the electrodes. The pure Photosystem II (PS II) cores from spinach immobilize onto the electrodes very efficiently but fair badly in terms of photocurrent response (measured using duroquinone as the redox mediator). The cruder preparation of PS II known as BBY particles performs significantly better under the same experimental conditions and shows a photocurrent response of 20 to 35 nA (depending on preparation) per screen-printed electrode surface (12.5 mm^2). The data was corroborated using AFM, showing that in the case of BBY particles a defective biolayer is indeed formed, with grooves spanning the whole thickness of the layer enhancing the possibility of mass transfer to the electrodes and enabling biosensing. In comparison, the PS II core layer showed ultra-dense organization, with additional formation of aggregates on top of the single protein layer, thus

[*] Corresponding author; phone (1-514) 848-2424 #5050; fax (1-514) 848-2828; e-mail: vzazubov@alcor.concordia.ca
[+]Present Address: Biosensors Laboratory, Institute of Microbial Technology, Sector 39-A Chandigarh India 160036; vkbhalla@imtech.res.in

blocking mediator access to the electrodes and/or binding sites. The defective monolayer biosensor with BBY particles was successfully applied for the detection of photosynthesis inhibitors, demonstrating that the inhibitor binding site remained accessible to both the inhibitor and the external redox mediator. Biosensing was demonstrated using picric acid and atrazine. The detection limits were 1.15 nM for atrazine and 157 nM for picric acid.

Keywords: Photosynthetic reaction centers; Gold screen printed electrode; Self-assembled monolayer; Herbicide detection; Atrazine; Picric acid.

* Corresponding author; phone (1-514) 848-2424 #5050; fax (1-514) 848-2828; e-mail: vzazubov@alcor.concordia.ca
+Present Address: Biosensors Laboratory, Institute of Microbial Technology, Sector 39-A Chandigarh India 160036; vkbhalla@imtech.res.in

1. Introduction

Biosensing, one of the many possible practical applications of biomolecules, requires the controlled immobilization of biomolecules in close contact with electrochemical transducers. Self-assembled monolayers (SAM) provide a unique tunable platform since the thickness of the organic layers and surface properties are adjustable to suit different sensing applications [1]. The organic molecules forming SAM feature different anchor groups that can be used to attach various classes of biomolecules [2]. They also provide some level of control over packing density at the surface [3]. Generally, use of SAMs allows the biochemical reaction to proceed in a more controlled manner thus enhancing biosensing parameters [4].

One common approach towards selective herbicide detection is based on the use of antibodies [5]. However, generation of antibodies against small molecules is tedious and time consuming process, and requires animal models to raise the antibodies. Antibody-based detection may also face problems due to cross-reactivity of antibodies with similar compounds [6]. Antibodies are fairly large objects, especially compared to small herbicide molecules; additionally, blocking in immunoassays is a complex problem that has to be addressed before any useful data is obtained. Summarizing, there is an apparent need to continue looking for alternative approaches, one of them being to employ the natural photosynthesis machinery for detection purposes. Photosynthetic biosensors are capable of detecting a broad spectrum of herbicides and have generated a lot of interest as an alternative to antibody-based biosensing. Whole photosynthetic organisms [7], as well as bacterial reaction centers [8], have been used for this purpose. The most common version makes use of Photosystem II (PS II), the photosystem that is also responsible for water splitting and oxygen production. The initial reports on PS II-based herbicide biosensors employed electrochemical flow cells with PS II in suspension [9] or

immobilized with the help of different substances [10-12]. Clark electrode-based setup that monitors changes in oxygen evolution activity of the PS II was used in [13]. More recent reports again focused on amperometric detection, with the photosynthetic material entrapped in gel matrices on top of the electrodes [14-17]. Combining electrochemical and optical detection has been recently reported in [18]. In PS II the illumination induces charge separation, with electron eventually traveling to mobile plastoquinone Q_B. In vivo the latter accepts two electrons (and two protons), transforms to quinol and carries the electrons away. The mechanism of inhibition of PS II by herbicides in vivo involves herbicide molecules attaching to the Q_B binding site and preventing plastoquinone from binding. The exposure of the PS II-based biosensor to the inhibitor results in a decrease of the photoinduced current in an electrical circuit containing the photosynthetic reaction centers, because the mediator (replacing plastoquinone) cannot bind to the Q_B site.

Although entrapping photosynthetic materials in gels allows for reasonable accessibility due to the porous nature of the matrix, it has some inherent limitations. The main limitations are due to swelling or contraction of gels with time, poor adhesion to the electrodes, and the stress of fluid movement that may lead to washing off of certain materials trapped in the matrix. The diffusion coefficient of mediators and herbicides in different gels, polymers and other matrices is also a limiting factor. Covalent immobilization using BSA-glutaraldehyde has been found to be better than other schemes as it is a simple one-step procedure based on cross-linking of amines that results in a very stable matrix system on top of the electrodes [16,18]. Another procedure, resulting in preservation of photosynthetic activity for somewhat longer time involves immobilization using poly(vinylalcohol) bearing styrylpyridinium groups (PVA-SbQ) [19].

The immobilization of photosynthetic materials in a monolayer fashion is quite challenging and has been of interest for various applications, including bioelectrocatalytic fuel cells [20]. The immobilization of PS II with the help of SAMs has been carried out using Histidine-tagged PS II that attaches to nickel on the NTA (nitrilotriacetic acid) SAM [21]. This technology requires genetic engineering to introduce the histidine tag into the PS II. Moreover, Ni-NTA-terminated SAM preparation on gold electrodes involves a multistep protocol. Thus, although this method leads to immobilization of the reaction centers in a uniformly-oriented fashion, the mass transfer to the electrodes becomes limited due to multiple layering steps effectively insulating the electrodes. Maly et al. [22] studied this topic and suggested deliberately creating defect structures using BSA in the PS II sensing biolayer to achieve increased mass transfer efficiency to the electrodes while working with NTA-SAM as the linker molecule. However, this approach could lead to decreased current due to the co-immobilization of BSA on the sensing surface.

In the present report we suggest a simpler approach that makes use of carboxylic acid anchoring groups of MPA SAM on gold screen-printed electrode (Au SPE) surface to bind native PS II reaction centers or membrane fragments for unique biointerface development. The MPA films are known to exhibit many pinhole defects [23]. We utilize these pinhole defects to achieve effective mass transfer to the electrodes.

2. Experimental

All chemicals were purchased from Sigma-Aldrich (USA). Organic baby spinach leaves were purchased from the local food suppliers. Buffer compositions were as follows:

Homogenizing buffer: 20 mM MES (pH 6.0), 15 mM NaC1, 5 mM $CaCl_2$. Measuring buffer: 15 mM 2-(N-morpholino) ethanesulfonic acid (MES), pH 6.5, 0.5 M mannitol, 0.1 M NaCl, 5 mM $MgCl_2$, and 5 x 10^{-5} M chloramphenicol (supplemented with 0.2 mM DQ).

2.1 Isolation of PS II-containing particles

The BBY particles [24] refer to PS II–enriched membrane fragments. The BBY particles are mostly devoid of Photosystem I, but still retain the oxygen evolving capacity and some lipid membranes within which the hydrophobic mediator can travel and reach its binding site. Both core and peripheral antenna complexes of PS II are retained. BBY particles were obtained after treatment of thylakoids with Triton X-100 at a final concentration of 25 mg per mg Chl and repeated centrifugation for 25 min at 40,000 g) in homogenizing buffer. The chlorophyll concentration for all purposes was determined by the method of Arnon [25].

The PS II core particles were prepared similarly to [26]. These particles constitute the minimal PS II preparation still retaining the oxygen-evolving capacity, and consist of the PS II reaction center, as well as CP43 and CP47 core antenna complexes. Note that in this case the photosynthetic protein is encased into the detergent micelle and the original thylakoid membrane is not retained.

2.2 Surface preparation procedures

A 2 mM MPA solution prepared in a 75/25% ethanol/water mixture (vol/vol) was used for the formation of SAMs. Gold surfaces were incubated for 1 hour, in the dark, and then rinsed with ethanol. After that sonication in ethanol/water was carried out for 5 minutes in order to remove physisorbed thiols from the gold surface. The surfaces were further washed with

deionized water and dried with nitrogen. For AFM investigations (see Sections 2.4 and 3.2), the SAM was formed not on a screen-printed electrode but on gold substrate (100 nm thickness) prepared by electron beam evaporation on a silicon dioxide chip with a 5 nm titanium stick layer. The gold surface was cleaned in a piranha solution (mixture of 3:1 of H_2SO_4 and H_2O_2) for 30 min before deposition of SAM.

After SAM formation, the electrodes were treated for 10 minutes with a mixture of NHS – N-hydroxysuccinimide (0.05 M) and EDC – Ethyl-Dimethyl-aminopropyl Carbodiimide (0.2 M) solutions in distilled deionized water. As a zero-degree cross-linking agent EDC does not introduce any additional chemical groups between the conjugating molecules**.** EDC reacts with carboxyl groups of the MPA SAM, forming an amine-reactive *o*-acylisourea intermediate. This intermediate in turn can react with amines of the photosynthetic material forming amide bonds and releasing isourea by-product [27]. A further incubation (6 hours at 4 °C in the dark) was carried out with the PS II particle suspension. The electrodes were carefully washed in MES buffer and dried with nitrogen after each incubation step.

2.3 Photo-electrochemical Measurements

Gold screen-printed electrodes were purchased from DropSens Inc. (model DRP-220. The electrode assembly consists of a gold working electrode (area 12.57 mm^2) and a gold counter electrode. The reference electrodes and electrical contacts were made of silver and screen printed on a ceramic substrate 3.4 x 1 x 0.05 cm (length x width x thickness). All potential values are reported with respect to silver pseudo reference electrode. The electrochemical

response of the electrodes with and without immobilized material was investigated using the CHI 630C electrochemical workstation.

The schematics of the biosensor are presented in Figure 1. For amperometric detection of photosynthesis inhibitors the *I-t* curves were measured at room temperature, with 50 µl droplets of the measuring buffer placed onto the working area covering the three electrodes. Duroquinone (DQ; 0.2 mM) was used as a mediator in these experiments and, respectively, the working electrode was polarized at 0.62 V [16,28]. Quinones are used as mediators in PS II-based herbicide biosensors due to their similarity to plastoquinone which binds to the Q_B site in vivo. DQ in particular was employed as a mediator also in [13,14,17]. Other mediators used in PS-II based biosensors include 2,5-dichlorobenzoquinone [11], 2,6-dichlorophenolindophenol [18] and ferricyanide [10,16,28]. Ferricyanide, although providing the largest photocurrents, is clearly not specific for the Q_B site [16,28]. A 7 mW laser diode with 675 nm wavelength (near the peak of the PS II Q_y absorption band) was used for illumination. In the absence of light only small dark current is registered. Illuminating the sensor leads to a significant increase in the detected current which is due to light-induced charge separation in the PS II. Turning the light off results in the return of the current to the pre-illumination levels (See also sections 3.1 and 3.3). Addition of photosynthesis inhibitors results in a decrease of the magnitude of the photo-induced current peak. [Suggested location of Fig.1)]

2.4 AFM Characterization

AFM studies were performed in order to assess the quality of SAM formation and photosynthetic material immobilization. The AFM images were obtained in air, while operating in tapping mode, using a Digital Instruments Multimode AFM with a standard sharpened Si_3N_4

tip (cantilever resonant frequency was 300 kHz). The images were collected with high resolution (512 points per line) at a scan rate of 1–2 Hz. Raw images were only processed for background removal (flattening) using the AFM manufacturer's software.

3. Results and Discussion

3.1 Electrochemical and photo-electrochemical characterization

The gold screen printed electrodes were used for thiol films formation. Not many reports have previously focused on thiol-Au films formation on screen printed electrodes; notable exceptions include [29,30]. Our goal was to form a non-insulating SAM (that would allow free movement of the mediator to the electrode surface) using short chain alkanethiols. It is well known that as the chain length decreases, the degree of order of SAM's decreases as well, together with the packing density and surface coverage [31]. The well-known redox curve of potassium ferrocyanide on gold electrode surface is presented in Figure 2 (solid curve). This curve can be compared with the curve measured for the electrodes covered with MPA SAM (dashed curve). The response is clearly decreased. On the other hand, the features of the cyclic voltammograms demonstrate that the thiol SAM is not perfectly insulating as the redox reaction of ferrocyanide is still accessible [32]. For comparison, almost no current is detected in case of highly-ordered SAM [33]. [Suggested location of Figure 2]

The proper immobilization of PS II core particles on MPA SAM was confirmed by observing the redox reaction for the various cofactors naturally present in the PS II structure. The cyclic voltammetry (CV) technique was used to characterize development of proper biointerface on SPE. The CV scans of immobilized core particles were obtained in MES buffer pH 6.5 and showed a reversible peak and a non-reversible peak when investigated using screen printed Au

electrodes with a silver pseudo-reference electrode (Supplemental Information, Fig. S1). A reversible peak at redox midpoint potential of –0.086 V can be ascribed to the (native) quinones (Q/Q^-), and the irreversible peak at ~0.22 V can be ascribed to the tetramanganese (Mn_4) cluster which shows that it is intact and accessible to the electrochemical reaction as described earlier [34]. The fact that this reaction is observed indicates close contact between PS II and the electrodes due to the short chain length of the SAM material.

Figure 3 compares the photocurrent signal measured as the reoxidation of the duroquinone (DQ) mediator at 0.62 V for the immobilized BBY sample in the cases of BSA-glutaraldehyde matrix system (A) and SAM (B), solid curves. The photocurrent signal is higher in case of SAM as compared to matrix-based immobilization for the same area of the electrode. As can be seen in the picture there is a significant difference in the sensor's response in these two cases. The difference arises mainly from the re-oxidation rate of the reduced mediator. In the case of immobilization of PS II on the SAM layer the mediator can access the electrode surface more easily. In the case of the matrix system, on the other hand, the speed of this process is limited by the diffusion rate of the mediator in the gel matrix and the reoxidation process takes longer [35]. The dotted curve in the frame B is an example of the signal in the presence of photosynthesis inhibitor. Surprisingly, the photocurrent signal in the case of PS II cores was 1.00 ± 0.75 nA only, significantly smaller than for BBY particles. [Suggested location of Figure 3]

Concerning the biosensor stability, in the case of BBY particles it took about 24 hours for the photocurrent signal to be reduced by half (see Supplemental Information, Fig. S2). The photocurrent did not show significant decay in the first 2 hours, most probably due to the stabilization effect of the natural lipid membrane environment.

3.2 Atomic force microscopy of surfaces

The photocurrent generation properties observed using duroquinone as a mediator were significantly different for BBY particles and PS II core preparations. AFM investigation allowed us to shed more light on the possible reasons of these differences. The AFM imaging was conducted using flat evaporated gold surface rather than the surface of the screen-printed electrodes. Thus, we managed to elucidate the fine details of SAM formation and photosynthetic material binding which could otherwise be partially masked by the higher surface roughness of the screen-printed electrodes. According to SEM images presented at manufacturer's website (http://www.dropsens.com), the surface of the screen-printed electrodes used in this work features granules of the size of ~ 2 μm, not very suitable for detailed AFM investigation. On the other hand, this is at least an order of magnitude larger than features described below. Thus, we believe that the details of SAM formation and PS II immobilization do not differ drastically between evaporated gold surface and screen-printed electrode. The quality of the SAM and of the bio-layer can be characterized by root mean square (RMS) roughness. Table 1 summarizes the RMS roughness values for bare surface as well as the surfaces after various modifications. The RMS roughness for the bare gold surface was 1.05 ± 0.1 nm. The deposition of the SAM led to a small increase in the surface roughness to 1.85 ± 0.25 nm. Figure 4 shows the AFM images of the bare gold surface and the MPA SAM on the gold surface. The topology of a nicely formed SAM almost perfectly follows the gold layer's corrugation, although defects in SAM such as cracks or patches would contribute to an increase in RMS roughness [36]. The immobilization of the photosynthetic complexes leads to a significant increase of the roughness. The RMS roughness increases to 21.9 nm with the immobilization of PS II core particles and to 8.67 nm for BBY membranes. The larger roughness in case of the pure PS II core sample is most

likely due to cluster formation as illustrated in the schematic accompanying Figure 5A. For BBY membranes we do not observe aggregate formation upon immobilization. The thickness of the layer is approximately 10 nm, in agreement with values previously reported for these particles using AFM imaging [22]. The AFM image of the immobilized PS II core particles on the MPA SAM (Figure 5A) show some repeatable features with the size (in the plane of the layer) of approximately 50 nm, as well as some objects of larger size, 100 nm and beyond. The height of the former features is approximately 10 nm. These must be the clusters of PS II core particles since individual PS II core dimers have been reported to have much smaller size, namely 20.6 x 13.1 nm, with thickness varying from 6.0 nm on the periphery of the complex to 9.1 nm in the RC region [37]. In [37] the thickness of the detergent layer around the hydrophobic surface of the protein was estimated at 1.6 nm only. Incidentally, in an earlier report the AFM images contained some 40-60 nm features for histidine-modified PS II immobilized on nickel-nitriloacetic acid (Ni-NTA) SAM [22]. Another report described smaller features whose size was consistent with that of the PS II dimers [38]. The high purity and homogeneity of this protein preparation allows immobilizing it in a very dense manner thus most likely completely blocking mediator access to the electrodes or the Q_B sites. (Although the PS II core samples were detergent-solubilized, one also cannot exclude a possibility that hydrophobicity of the complexes, isolated from natural membranes, contributes to their aggregation.) This result is in accordance with those by other researchers who found higher protein densities to interfere with biosensor assays mainly by interfering with the diffusion of the analyte to the enzyme or by hindering electron transfer to the electrode surface [39]. In addition, higher protein loading on the surface, particularly for enzymes, has been shown to neutralize active sites or alter the morphology of the enzyme through mutual interactions [40]. Thus, the poor performance of this

preparation, in our case, was ascribed to the higher protein density, in agreement with the results of other researchers who found high protein densities to be a limiting factor in the performance of biosensors [41-43]. It is also possible that detergent micelle, as opposed to native thylakoid membrane present in BBY particles, is preventing the access of the mediator to the Q_B site.

In the case of BBY particles the membrane fragments successfully immobilize on the surface but not in an ultra-dense manner. The image in Figure 5B shows heterogeneous features. It has both areas (marked with a square) with uniform immobilization of relatively small membrane fragments, as well as regions (outside of the square) with large membrane fragments on top of the gold surface and possibly on top of each other. The presence of the natural membrane environment in case of BBY particles likely allows the hydrophobic mediator to gain better access to the Q_B binding site. The presence of nanogaps in the film allows the reduced mediator in solution to gain better access to the electrode surface as shown in schematic accompanying Figure 5B. The smallest particles present in the AFM image in Figure 5B appear to be approximately 25-30 nm, consistent with the size of the dimeric PS II supercomplexes containing peripheral antenna [37]. Figure 6 directly compares the cross-section features (along the lines present in Figure 5 A and B, respectively) for the two sample preparations. In case of the PS II cores the features repeat with the period of approximately 100 nm, with occasional larger aggregate formation. In case of BBY sample the grooves are observed in the biolayer, spanning the total thickness of the biolayer i.e. ~10 nm. Thus in the latter case there is ample opportunity for mediator to gain access to the electrode surface. [Suggested location for Figures 4, 5, 6]

3.3 Detection of photosynthesis inhibitors

Herbicides inhibit photosynthesis by interrupting electron transfer at the quinone-reducing site of PS II. In vivo herbicides compete with the plastoquinone for its Q_B binding site on the D1 protein, thus leading to disruption of electron transfer from Q_A to Q_B and further along the electron transport chain. In our experiments the herbicide binding to the Q_B site did not allow the mediator (DQ) to accept electrons from the site and hence the process of electron transfer from PS II to the mediator and further to the electrode was stalled. The detection was based on the decrease in photocurrent in the presence of herbicides (see Frame B of Figure 3).

Reference photocurrent was first obtained without the addition of herbicides. A preconditioning phase of about 10 minutes was required before the photocurrent from a fresh biosensor became stable. A droplet (50 µl) of measuring buffer containing the mediator was allowed to spread over the electrodes covered with immobilized PS II and the photocurrent generated from the biosensor was measured for illumination time of 10 s~~ec~~ after 10 min of incubation. The biosensor was then subjected to successive droplets containing increasing concentrations of the herbicide and the light-induced current was measured, again after 10 min of incubation. In between applying different herbicide concentrations the sensor surface was washed with excess of measuring buffer (including DQ) to remove the herbicide. Each measurement was recorded three times at the same concentration of the analyte (using fresh droplets) to check for reproducibility.

The data for different analytes was plotted as residual activity versus concentration (on a logarithmic scale), Figure 7. The residual activity is the activity of the biosensor in percent after addition of the inhibitor; it is equal to the ratio of photocurrents in the presence and in the absence of the inhibitor. Experimental data were fitted to a logistic equation describing a sigmoidal binding curve.

$$R = \min + \frac{Max - Min}{1 + (x / IC50)^{H}} \quad (1)$$

Here *Max* is the maximal activity before adding any analyte and *Min* is the minimum residual activity, when sensor is saturated by the inhibitor; *H* is the Hill slope, and x is the inhibitor concentration. The *IC50* is the point midway between top and bottom of the sigmoidal curve. The assumption behind the use of this curve is that the mediator and the inhibitor bind competitively to one and the same site on the PS II. The limit of detection, LOD, was calculated as

$$LOD = IC50\left(\frac{2.6\sigma}{Max - Min - 2.6\sigma}\right)^{1/H} \quad (2)$$

see [28]. The factor of 2.6 corresponds to 99% confidence interval. Picric acid can be classified as nitrophenolic herbicide according to its chemical structure and has been employed in research on the feasibility of the PS II-based biosensors for explosives detection [28]. It has been previously described to be an inhibitor of PS II in photosynthetic electron transport [44]. The curve shifts towards higher concentrations for the picric acid in comparison to atrazine, indicating a lower degree of picric acid binding to the Q_B site. The fit parameters are presented in Table 2. The IC_{50} for picric acid is 15 times higher as compared to atrazine which signifies a lower affinity of picric acid for the Q_B binding site in comparison to triazine-type herbicides. The developed assay showed an excellent dynamic response range between 1 nM to 1 µM for detection for atrazine and LOD is 1.15 nM indicating its potential application for environmental analysis. In repeated experiments, the reproducibility (coefficient of variation) of the sensor for n=3 measurements was ~5 %, for 10 nM atrazine concentration. The LOD of different atrazine sensors reported in the literature are summarized in Table 3. The limit of detection of 1.15 nM

for atrazine is significantly lower than the Maximum Residue Level (MRL) (50 µg L^{-1} or 232 nM) established by EU (European Union) and close the MRLs for drinking water of each individual pesticide at 0.1 µgL^{-1} and the total amount of pesticides at 0.5 µg L^{-1} (2.32 nM). [Suggested location of Figure 7] For picric acid the sensor shows a relatively poor LOD of 157 nM which is mostly attributable to high σ. The LOD of ~25 nM has been reported for BSA glutaraldehyde gel-immobilized PS II picric acid biosensor in [28]. The luminescence quenching method yields LOD of 2 µM [45]; employing the fluorescence emission of hexaphenysilole-chitosan film the LOD of ~21 nM can be achieved [46]. It is important to point out that just like most reported PS II-based herbicide biosensors [12,16,28], the one reported in this work is not capable of distinguishing between different inhibitors without *a priori* knowledge of either the nature of an inhibitor or the concentration. Thus, in its present form the biosensor is most suitable for non-selective early-warning type applications. However, the use of genetically modified PS II promises to allow better selectivity [18].

The main advantage of using SAM as compared to a matrix system is that due to smaller biomolecule-to-electrode distance and to the absence of matrix which slows down the diffusion of both analyte and the mediator, the equilibration and response times as well as the recovery times are decreased, leading to lower illumination time being necessary. The peak response at complete inhibition is near zero. It is possible to completely restore the signal by washing the sensor with measuring buffer. The regeneration of the biosensor after experiments was almost 100% effective, in agreement with the results of [16]. It is also possible to reuse this sensor after storage at 4º C within several hours, although within 24 hours the current drops substantially. Longer-time storage of prepared sensors without loss of activity is possible at –80º C.

Conclusions

This paper investigates a method for covalent immobilization of photosynthetic reaction centers on top of a defective self-assembled monolayer that allows mediator to access the surface of the electrodes easily. The photocurrent generation properties in case of BBY particles were compared to results obtained with BSA-glutaraldehyde matrix based immobilization and they show faster rise and decay of the photocurrent upon switching illumination on and off, and better signal to noise ratio. The pure preparations of Photosystem II cores (with no lipids) from spinach leaves immobilize very nicely on the electrode surface but fair badly in terms of photocurrent generation properties. The AFM investigations helped us to better understand some of the obtained results as we see that BBY particles organize themselves into a layer structure on top of the SAM leaving certain free spaces. The PS II core preparation in turn shows a very dense organization with aggregate formation that leaves no space for mediator to access the electrodes. The action of photosynthesis inhibitors in reducing photo-induced current was demonstrated for atrazine and picric acid. The obtained detection limits were 1.15 nM and 157 nM, respectively.

Acknowledgments:

Authors are thankful to Dr. Rolf Schmidt, facility manager, Concordia University, for his help in acquisition of AFM images and to Dr. C. Raman Suri (Pesticide Biosensors group) of IMTECH Chandigarh, for fruitful discussions. The funding has been provided by NSERC under Strategic Grants Program, Safety and Security. We acknowledge Defense R&D Canada, RCMP, CBSA and CATSA as supporting organizations.

References

1. Z. Dai, H. Ju, Phys. Chem. Chem. Phys. 3 (2001) 3769-3773.
2. N.K. Chaki, K. Vijayamohanan, Biosens. Bioelectron. 17 (2002) 1–12.
3. S. Ferretti, S. Paynter, D.A. Russell, K.E. Sapsford, D.J. Richardson, Trends Anal. Chem. 19 (2000) 530-540.
4. F. Frederix, K. Bonroy, W. Laureyn, G. Reekmans, A. Campitelli, W. Dehaen, G. Maes, Langmuir 19 (2003) 4351–4357.
5. C.R. Suri, R. Boro, Y. Nangia, S. Gandhi, P. Sharma, N. Wangoo, K. Rajesh, G.S. Shekhawat, Trends Anal. Chem. 28 (2009) 29-39.
6. B. Byrne, E. Stack, N. Gilmartin, R.O. Kennedy, Sensors, 9 (2009) 4407-4445.
7. I. Shitanda, S. Takamatsu, K. Watanabe, M. Itagaki, Electrochim. Acta. 54 (2009) 4933–4936.
8. H. Peters, C.S. Dannert, R D. Schmid. Mater. Sci. Eng. C 4 (1997) 227-232.
9. S. Lemieux, R. Carpentier, J. Photochem. Photobiol. B 2 (1988) 221-231.
10. S. Lemieux, R. Carpentier, Photochem. Photobiol. 48 (1988) 115-121.
11. C. Loranger, R. Carpentier, Biotechnol. Bioeng. 44 (1994) 178-183.
12. D. Laberge, J. Chartrand, R. Rouillon, R. Carpentier, Env. Toxicol. Chem. 18 (1999) 2851-2858.
13. M. Koblízek, J. Masojídek, J. Komenda, T. Kucera, R. Pilloton, A. K. Mattoo, M. T. Giardi, Biotech. Bioeng. 60 (1998) 664-669.
14. F. Bettazzi, L. Laschi, M. Mascini, Anal. Chim. Acta 589 (2007) 14–21.
15. E. Touloupakis, L. Giannoudi, S.A. Piletsky, L. Guzzella, F. Pozzoni, M.T. Giardi, Biosens. Bioelectron. 20 (2005) 1984–1992.

16. M. Koblízek, J. Maly, J. Masojídek, J. Komenda, T. Kucera, M.T. Giardi, A.K. Mattoo, R. Pilloton, Biotechnol. Bioeng. 78 (2002) 110-116.
17. A. Tibuzzi, G. Pezzotti, T. Lavecchia, G. Rea, M. T. Giardi, Sens. Transducers 88 (2008) 9.
18. K. Buonasera, G. Pezzotti, V. Scognamiglio, A. Tibuzzi, M.T. Giardi, J. Agric. Food Chem. 58 (2010) 5982-5990.
19. E.V. Piletskaya, S.A. Piletsky, T.A. Sergeyeva, A.V. El'skaya, A. A. Sozinov, J.L. Marty and R.Rouillon, Anal. Chim. Acta 391 (1999) 1–7.
20. K.B. Lam, E.F. Irwin, K.E. Healy and L. Lin, Sens. Act. B Chem. 117 (2006) 480-487.
21. N. Terasaki, M. Iwai, N. Yamamoto, T. Hiraga, S. Yamada, Y. Inoue, Thin Solid Films 516 (2008) 2553–2557.
22. J. Maly, J. Krejci, M. Ilie, L. Jakubka, J. Masojidek, R. Pilloton, K. Sameh, P. Steffan Z. Stryhal, M. Sugiura. Anal. Bioanal. Chem. 381 (2005) 1558–1567.
23. S. Campuzano, M. Pedrero, C. Montemayor, E. Fatas, J.M. Pingarron, J. Electroanal. Chem. 586 (2006) 112–121.
24. D.A. Berthold, G.T. Babcock, C.F. Yocum, FEBS Lett. 134 (1981) 231.
25. D.I. Arnon, Plant Physiol. 24 (1949) 1-15.
26. P.J. van Leeuwen, M.C. Nieveen, E.J. van de Meent, J.P. Dekker, H.J. Gorkom, Photosyn. Res. 28 (1991) 149-153.
27. T. Hermanson, In: Bioconjugate Techniques, Academic Press, San Diego, CA, 1996, pp. 139–140.
28. V. Bhalla, X. Zhao, V. Zazubovich, J. Electoanal. Chem. 657 (2011) 84-90.
29. J. Shen, C.C. Liu, Sens. Actuators B: Chem. 120 (2007) 417-425.
30. O.A. Loaiza, S. Campuzano, M. Pedrero, J.M. Pingarron, Electroanal. 20 (2008) 1397–1405.

416 31. C.D. Bain, E.B. Troughton, Y.Y. Tao, J. Evall, G.M. Whitesides, R.G. Nuzzo, J. Am. Chem.
417 Soc. 111 (1989) 321-335.
418 32. V. Anandan, R. Gangadharan, G. Zhang, Sensors 9 (2009) 1295-1305.
419 33. V. Bhalla, S. Carrara, C. Stagni, B. Samorì, Thin Solid Films 518 (2010) 3360-3366.
420 34. Alcantara, B. Munge, Z. Pendon, H.A. Frank, J.F. Rusling, J. Am. Chem. Soc. 128 (2006)
421 14930–14937.
422 35. J. Maly, A. Masci, J. Masojidek, M Sugiura, R. Pilloton, Anal. Letts. 37 (2004) 1645-1656.
423 36. S. Carrara, V. Bhalla, C. Stagni, B. Samorì, Surf. Sci. 603 (2009) 75–77.
424 37. E. J. Boekma, B. Hankamer, D. Bold, J. Kruip, J. Nield, A. F. Boonstra, J. Barber, M.
425 Rogner, Proc. Natl. Acad. Sci. USA 92 (1995) 175-179.
426 38. A. Morrin, A. Guzman, A. J. Killard, J. M. Pingarron, M. R. Smyth, Biosens. Bioelectron. 18
427 (2003) 715–720.
428 39. M. Vittadello, M.Y. Gorbunov, D.T. Mastrogiovanni, L.S. Wielunski, E.L. Garfunkel, F.
429 Guerrero, D. Kirilovsky, M. Sugiura, A.W. Rutherford, A. Safari, P.G. Falkowski,
430 ChemSusChem 3 (2010) 474-475.
431 40. R. Ganapathy, S. Manolache, M. Sarmadi, W. J. Simonsick Jr., F. Denes, J. Appl. Polym.
432 Sci. 78 (2000) 1783–1796.
433 41. Z. Naal, J.H. Park, S. Bernhard, J.P. Shapleigh, C.A Batt, H.D. Abrua, Anal. Chem. 74
434 (2002) 140–148.
435 42. R.D. Richins, A. Mulchandi, W. Chen. Biotechnol. Bioeng. 69 (2000) 591–596.
436 43. M. Darder, E. Casero, F. Pariente, E. Lorenzo, Anal Chem. 72 (2000) 3784–3792.
437 44. W. Oettmeier, K. Masson, Eur. J. Biochem. 122 (1982) 163-167.
438 45. J. Lu, Z. Zhang, Anal. Chim. Acta. 318 (1996) 175.

439 46. G. He, H. Peng, T. Liu, M. Yang, Y. Zhang, Y. Fang, J. Mater. Chem. 19 (2009) 7347.
440 47. S. Hleli, C., Martelet, A. Abdelghani, N. Burais, N., Jaffrezic-Renault, Sens. Actuators B 113
441 (2006) 711–717.
442 48. E. Valera, J. Ramón-Azcón, F.-J. Sanchez, M.-P. Marco, Á. Rodríguez, Sens. Actuators B
443 134 (2008) 95-103
444 49. J. Přibyl, M. Hepel, J. Halamek, P. Skladal, Sens. Actuators B 91 (2003) 333–341.
445 50. C. Steegborn, P. Skladal, Biosens. Bioelectron. 12 (1997) 19-27.
446 51. C.R. Suri, J. Kaur, S. Gandhi, G.S. Shekhawat, Nanotechnology 19 (2008) 235502.
447 52. R. Wilson, M.H. Barker, D.J. Schiffrin, R Abuknesha, Biosens. Bioelectron. 12 (1997) 277–
448 286.
449 53. J. Kaur, R.C.Boro N. Wangoo, K. Rajesh, C.R. Suri, Anal. Chim. Acta. 607 (2008) 92-98.
450

Figure Captions

Figure 1. Schematics of the biosensor employed in this work. PS II-containing particles are immobilized on top of a defective monolayer of MPA on a gold electrode. Light induces charge separation in PS II and after several steps the electrons are accepted at the Q_B binding site by a non-native quinone (duroquinone, DQ) The reduced DQ leaves the Q_B site and is eventually oxidized at the gold SPE and the photo-induced current is detected. Introduction of photosynthesis inhibitors interrupts this chain of events and the photoinduced current is reduced.

Figure 2. CV scans obtained using 30 mM ferrocyanide in measuring buffer (no DQ) for bare Au-SPE (solid curve) and after MPA SAM formation (dashed curve). The scan rate was 50 mV s~~ec~~$^{-1}$.

Figure 3. Comparison of photocurrent signal from BBY particle biosensor in case of (A) BSA-glutaraldehyde matrix immobilization and (B) immobilization onto a self-assembled MPA monolayer in the absence of inhibitors, solid curves. The illumination time is 20 s~~ec~~ for (A) and 10 s~~ec~~ for (B). The dotted curve in frame B is the photocurrent peak in the presence of an inhibitor, superimposed on the figure for illustrative purposes.

Figure 4. AFM images. Square side is 5.0 μm^2. a) Bare gold surface and b) Gold surface after formation of MPA SAM. In the image (b), the brighter regions correspond to the condensed thiol islands (liquid or solid phase), and the darker regions correspond to the dilute phase (bare Au surface).

Figure 5. AFM images of PS II particles immobilized on a MPA monolayer; square size 2.5 μm^2. a) PS II cores from spinach. Immobilized particles show cluster formation thus blocking mediator access to the electrode surface; b) BBY particles: immobilized particles as well as access sites to electrodes are visible. The RMS roughness in the highlighted square region is 4.16 nm. Below the AFM images the respective schematic drawings of the biolayers are presented.

Figure 6. Cross-sectional views along the lines present in Figure 4. a) PS II core particles are located right next to each other and some aggregates are formed. b) Highly disordered situation in case of BBY membranes, with grooves clearly spanning the whole thickness of the biolayer.

Figure 7. Calibration curves for the decrease of photocurrent upon addition of picric acid (open circles) and atrazine (solid circles) in the presence of 0.2 mM DQ. The experimental points were fitted using Eq.1.

Table 1. RMS roughness for various samples/surfaces

Sample	RMS roughness in nm for 2.5 μm^2 square
Bare evaporated gold	1.05 ±0.1
MPA-SAM	1.85 ± 0.25
PS II cores	21.9
BBY	8.67

Table 2. Fitting parameters (Eqs. 1 and 2) for picric acid and atrazine

	Min (%)	Max (%)	EC50 (nM)	σ	Hill slope	R^2	LOD (nM)
atrazine	7.6	100.0	49	1.57	0.82	0.9984	1.15
picric acid	10.4	100.0	784	4.83	1.13	0.9936	157.5

Table 3. **Examples of atrazine biosensors**

Ref.	Methodology	LOD
[47]	Impedimetric, label-free immunosensor	20 ng/ml 93 nM
[48]	Impedimetric, label-free immunosensor	8.34±1.37 ng/ml 39 nM
[49]	Piezoelectric, label-free immunosensor	1.5 ng/ml (direct) 7 nM / 0.025 ng/mL (competitive) 0.11 nM
[50]	Piezoelectric	0.1 μg/l 0.46 nM
[51]	Nanomechanical Cantilever based	pM
[52]	Electrochemiluminescence flow injection immunoassay	0.1 ppb 6 nM
[53]	Direct hapten coatin microtiter plates	20 ng/L 0.09 nM
This work	PSII biosensor	247 ng/L 1.15nM

Figure

Click here to download high resolution image

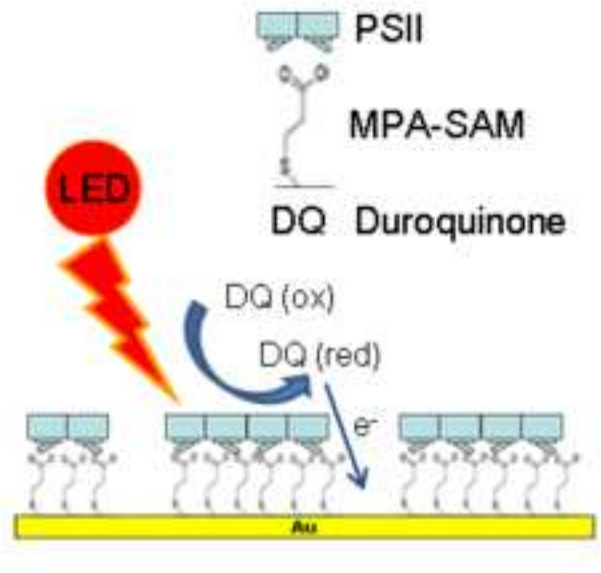

Figure

Click here to download high resolution image

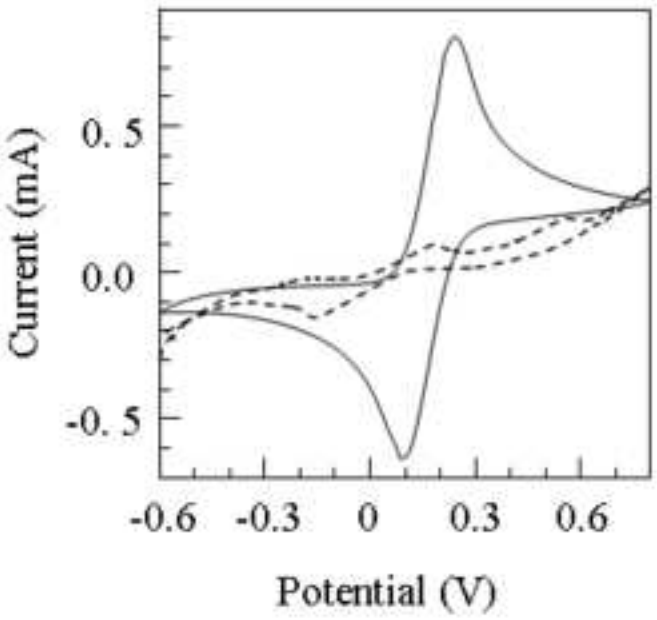

Figure 2

Figure
Click here to download high resolution image

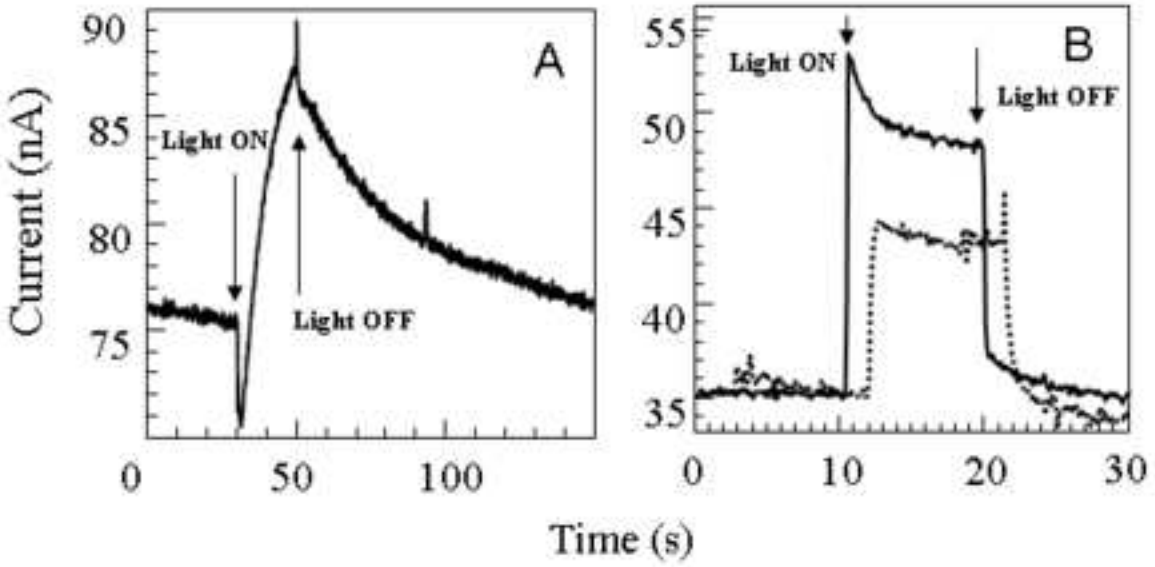

Figure 3

Figure
Click here to download high resolution image

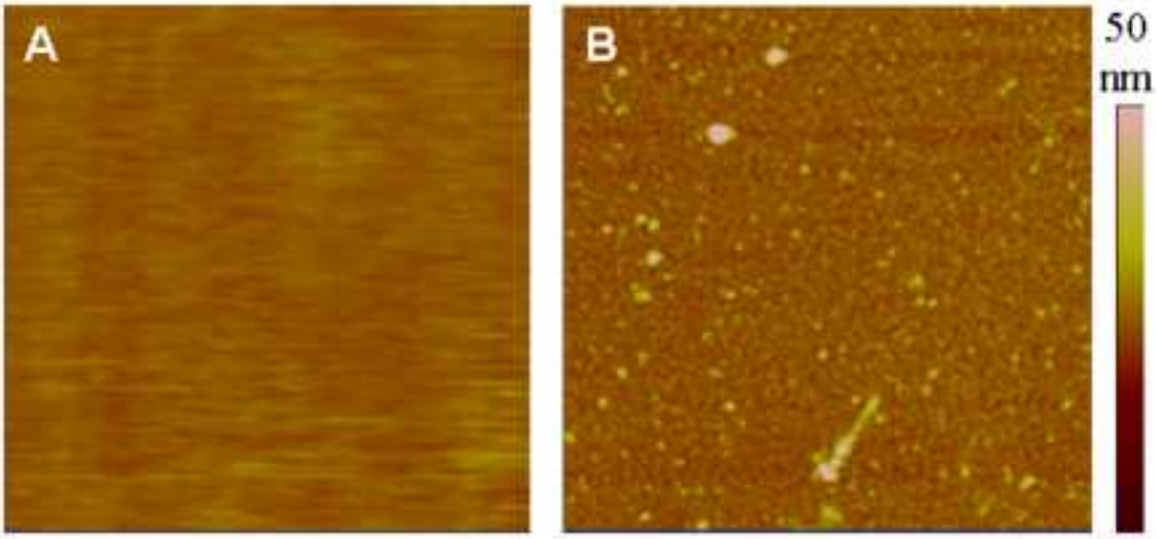

Figure 4

Figure
Click here to download high resolution image

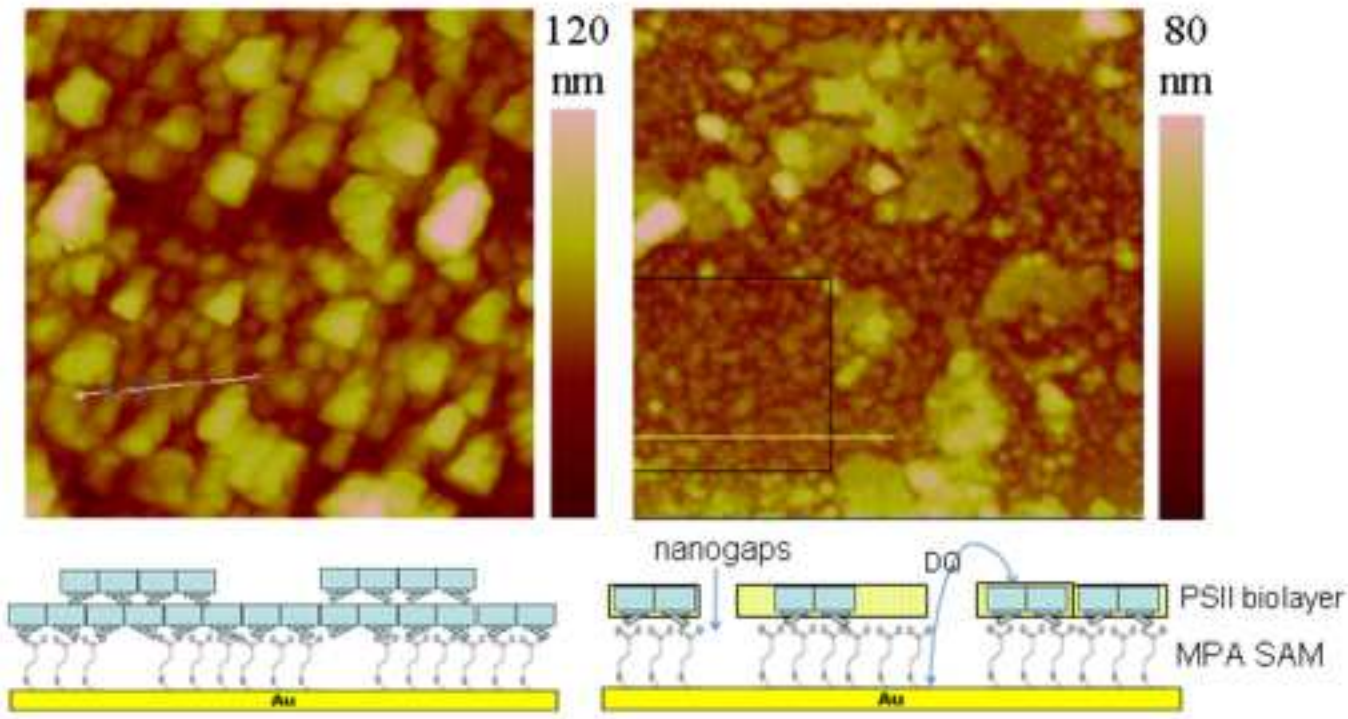

Figure 5

Figure

Click here to download high resolution image

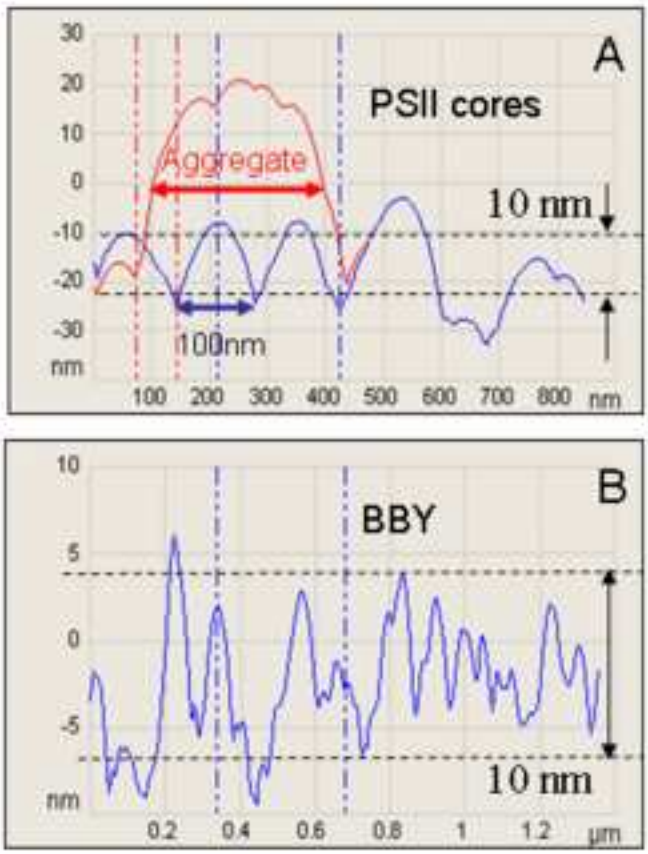

Figure 6

Figure

Click here to download high resolution image

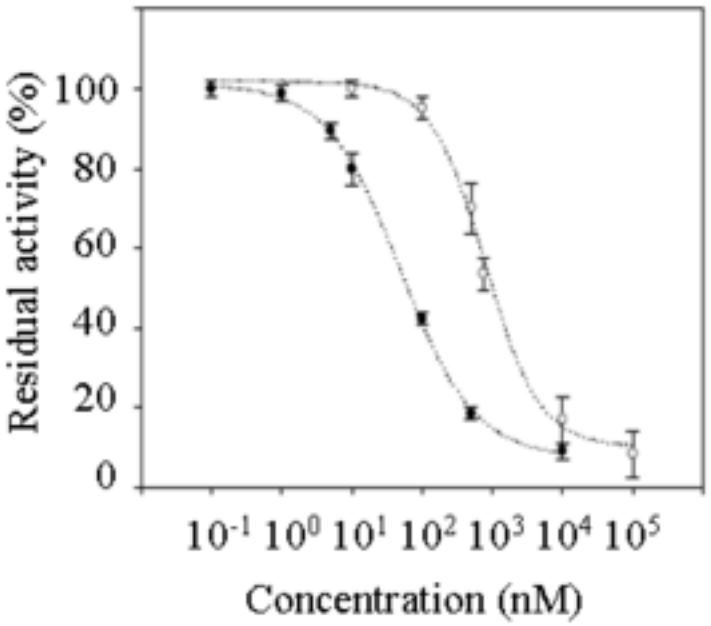

Figure 7

Electronic Supplementary Material (online publication only)

Click here to download Electronic Supplementary Material (online publication only): Supplementary Information.doc